ACS OMEGA

Open Access

http://pubs.acs.org/journal/acsodf

Article

CIELAB Color Space as a Field for Tracking Color-Changing Chemical Reactions of Polymeric pH Indicators

Takayuki Suzuki,* Chihiro Ito, Karen Kitano, and Tomohiro Yamaguchi

Cite This: *ACS Omega* 2024, 9, 36682−36689

Read Online

ACCESS | Metrics & More | Article Recommendations | Supporting Information

ABSTRACT: Two types of cross-linked polymeric dye films that exhibit reversible color changes in response to pH were prepared. Upon protonation, films with a nitrophenol dye moiety (NP) changed from yellow to colorless, whereas films with an azobenzene dye moiety (AB) changed from yellow to reddish-purple. The colored light transmitted through these films from a D65 white-light source was measured colorimetrically, and the transition of the chromaticity point in CIELAB upon protonation of the polymeric dyes was observed. At low dye concentrations ([NP] < 4.7×10^{-5} and [AB] < 2.7×10^{-5} mol L^{-1}), linear loci of the chromaticity points were displayed for both polymeric dye films, indicating perceptual linearity. This linearity is caused by the avoidance of nonlinear perceptual phenomena such as the Abney effect and the Bezold−Brücke phenomenon. The perceptual linearity of space is a necessary condition for achieving stoichiometric linearity, which requires an additional linear relationship between the dye concentration and each component, a^*, b^*, and L^*. A geometric equation that included the AB concentration and the protonation ratio of AB was used to successfully depict, on the basis of stoichiometric linearity, the protonation of the polymeric AB films three-dimensionally in the restricted area of CIELAB.

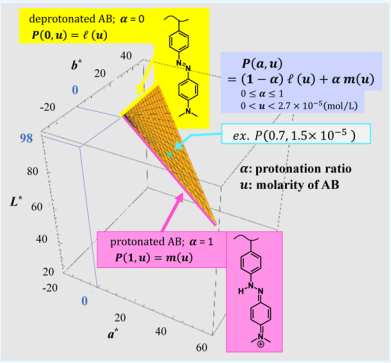

INTRODUCTION

Many researchers have used imaging devices such as scanners and digital cameras to measure the color change of indicators and convert it into perceptual color information for quantification to detect target substances[1,2] such as metal ions[3−7] and gases,[8,9] as well as pH.[10−14] Color information is generated using three-axis variables in a three-dimensional (3D) color space. Color spaces include the HSV,[4,5,11,14] CIE RGB,[6,8,15] CIE XYZ,[12,13] and CIELAB color spaces.[3,7,10]

Some CIE color spaces that exhibit perceptually high uniformity of color have historically been proposed.[16] CIEW*U*V*,[17] CIELUV,[18] and CIELAB are representatives of these color spaces. The CIELAB color space is often used to quantify colored chemicals.[19,20] The chromaticity point, as the color information on indicators, includes three variables in the CIELAB color space: a^*, b^*, and L^*. The perceptual color difference between two different chromaticity points, which varies with color-changing indicators, is represented in the CIELAB color space by ΔE^*_{ab}, which is the Euclidean distance between chromaticity points (eq 1).[7,21] The amount of the color-changing indicators has been determined using calibration curves that relate the concentration of the indicator to its ΔE^*_{ab}[3,7,10] because the ΔE^*_{ab}-based perceptual linearity in the CIELAB color space does not necessarily coincide with stoichiometric linearity.

$$\Delta E^*_{ab} = \sqrt{(\Delta a)^2 + (\Delta b)^{*2} + (\Delta L)^{*2}} \quad (1)$$

By contrast, according to the Lambert−Beer rule, absorption spectra demonstrate a proportional relationship between the molar concentration of a dissolved substance and the absorbance in dilute solutions.[22] This important relationship means that absorption spectra can be used not only to quantify substances but also to track the behavior of chemical reactions. If the CIE color space is equipped with a limited range that ensures stoichiometric linearity, it can serve as a field that allows tracking of chemical reactions by visual depiction using a 3D color-coded perspective.

The chromaticity point for a transmitted color from a white-light source through a colorless transparent object has a lightness L^* equal to 100 in the CIELAB color space, and the other two variables indicating hue, a^* and b^*, are zero; that is, the white point is $(a^*, b^*, L^*) = (0, 0, 100)$. The preparation of a sufficiently dilute solution of a colored substance provides a solution chromaticity point located near the white point. Perceptual linearity by ΔE^*_{ab} in CIELAB is preferred in this region.[3] Object colors with high lightness are perceived predominantly by the three types of cones in the human eye. As lightness decreases, only one type of rod, which is highly

Received: June 6, 2024
Revised: August 2, 2024
Accepted: August 6, 2024
Published: August 15, 2024

https://doi.org/10.1021/acsomega.4c05320
ACS Omega 2024, 9, 36682−36689

sensitive to a specific color, is added to perception. The Bezold−Brücke phenomenon at low lightness and the Abney effect at high saturation cause nonlinear perceptual phenomena.

The region near the white point, where such perception-specific phenomena are unlikely to occur, should be more applicable for stoichiometric quantification of substances. Yellow 5Y in the hue for the Munsell color system[23] is relatively resistant to the Abney effect and lightness (value) reduction, even when its saturation (chroma) increases with increasing color density. Ohta used dyes with three basic colors (yellow, magenta, and cyan), measured the color resulting from stepwise changes of the dyes' concentrations, and reported the trajectory of the chromaticity points in the CIE 1931 chromaticity diagram.[24] Yellow indicates a large ΔE^*_{ab} resulting from large saturation changes, even in the low dye concentration range, supporting a highly accurate quantification.

Conventional low-molecular-weight dyes require the preparation of a sample for each pH measurement. Polymeric dyes, in which the dye moiety is covalently fixed in the film, are suitable for the long-term continuous observation of the same film. Herein, we report color changes of two types of polymeric dyes upon protonation (pH change) in the CIELAB color space. One is polymeric nitrophenol (NP), which reversibly changes from colorless to yellow in response to a change in pH. The other is polymeric azobenzene (AB), which shows a reversible change between different colors (yellow and red-purple) in response to a change in pH. The single-color shade in the NP dye is easy to quantify using a single variable that exhibits the widest variation,[19] whereas quantification by mixing multiple colors requires all three variables (a^*, b^*, and L^*) of the CIELAB color space to be captured in a case such as the AB dye.[10] In the present study, we evaluate the CIELAB color space as a potential field for tracking the protonation reaction of polymer pH indicators.

MATERIALS AND METHODS

Materials. *N*-Isopropylacrylamide was purchased from FUJIFILM Wako Pure Chemical and was purified by recrystallization from a mixture of benzene and *n*-hexane. Other reagents were used as received without any processing.

Synthesis of Dyes. *N*-(2-Hydroxy-5-nitrobenzyl)-acrylamide was prepared by reacting 4-nitrophenol (2.78 g) with *N*-(hydroxymethyl)acrylamide (1.00 g) at 40 °C in trifluoroacetic acid (15.0 mL) with phenothiazine (1.00 mg) as a polymerization inhibitor for 14 h. The solution was added to chloroform, followed by the addition of hydrochloric acid, and the organic layer was extracted. The product was purified by column chromatography with a mixture of *n*-hexane and ethyl acetate (v/v = 7:3) as a developing solvent to give *N*-(2-hydroxy-5-nitrobenzyl)acrylamide (NP, R_f = 0.23): yield 0.74 g (33%); mp 132−133 °C; ^{1}H NMR (400 MHz, DMSO-d_6) δ 8.66 (s, 1H), 8.04 (m, 2H), 7.00 (d, 1H), 6.32 (dd, 1H, J = 10.4, 18.0 Hz), 6.16 (dd, 1H, J = 2.0, 17.2 Hz), 5.67 (dd, 1H, J = 2.4, 10.4 Hz), 4.34 (d, 2H).

(*E*)-4-((4-Bromophenyl)diazinyl)-*N*,*N*-dimethylaniline was prepared by mixing 4-bromoaniline (1.0 g) was mixed with an aqueous solution of sodium nitrite (0.6 g/1.0 mL of H_2O) in hydrochloric acid (HCl, 35 wt %, 0.8 mL). The mixture was then reacted with *N*,*N*-dimethylaniline (1.48 mL) in acetic acid (99.5%, 2.7 mL) at 0 °C for 5 h. The solution was subjected to phase separation using chloroform and water. The organic layer was extracted and subsequently purified by column chromatography with chloroform as a developing solvent to give (*E*)-4-((4-bromophenyl)diazinyl)-*N*,*N*-dimethylaniline (R_f = 0.64): yield 0.68 g (39%); mp 154−155 °C; ^{1}H NMR (400 MHz, $CDCl_3$) δ 7.89 (d, 2H), 7.74 (d, 2H), 7.61 (d, 2H), 6.78 (d, 2H), 3.12 (s, 6H).

(*E*)-*N*,*N*-Dimethyl-4-((4-vinylphenyl)diazinyl)aniline was prepared by reacting (*E*)-4-((4-bromophenyl)diazinyl)-*N*,*N*-dimethylaniline (0.70 g) with 4,4,5,5-tetramethyl-2-vinyl-1,3,2-dioxaborolane (0.60 mL) at 100 °C for 24 h in a mixture of 1,4-dioxane (4.5 mL) containing cesium carbonate (1.6 g) and water (4.5 mL) containing tetrakis(triphenylphosphine) palladium(0) (0.076 g). The solution was poured into water, and the aqueous layer was extracted with chloroform. The organic layer was separated, followed by column chromatography with chloroform as a developing solvent to give (*E*)-*N*,*N*-dimethyl-4-((4-vinylphenyl)diazinyl)aniline (AB, R_f = 0.54): yield 0.51 g (92%); mp 162−163 °C; ^{1}H NMR (400 MHz, $CDCl_3$) δ 7.90 (d, 2H), 7.83 (d, 2H), 7.53 (d, 2H), 6.78 (m, 1H), 6.78 (d, 2H), 5.84 (d, 1H), 5.33 (d, 1H), 3.12 (s, 6H).

Synthesis and Characterization of Polymer Dyes. A polymer dye carrying an NP or AB moiety as a monomeric pH indicator was prepared by copolymerization of NP (13.6 mg) or AB (15.5 mg) and *N*-isopropylacrylamide (0.68 g) with azobis(isobutyronitrile) (12 mg) as an initiator in dimethyl sulfoxide (DMSO) (3.0 mL) at 60 °C for 8 h.

^{1}H NMR spectra were recorded on a Bruker AVANCE III HD 400 spectrometer operating at 400 MHz for the polymer dye of NP or AB to determine the dye contents: NP, 0.5 mol %; AB, 1.6 mol %. The ultraviolet−visible (UV−vis) absorption spectra of the aqueous solution of the polymer dye were acquired at room temperature using an Agilent 8453 diode-array spectrophotometer. The molar extinction coefficient of the NP portion in the polymer NP at 420 nm in an alkali solution at pH 11 was 1.3×10^4 L mol^{-1} cm^{-1}, and that of the AB portion in the polymer AB at 520 nm in an acidic solution at pH 0.5 was 2.3×10^4 L mol^{-1} cm^{-1}. Several buffer solutions of the polymer NP with different NP concentrations (1.2×10^{-5}, 2.3×10^{-5}, 4.7×10^{-5}, 9.4×10^{-5}, and 1.3×10^{-4} mol L^{-1} of the NP segment) were prepared. Buffer solutions of the polymer AB were similarly prepared: 3.1×10^{-6}, 6.2×10^{-6}, 1.3×10^{-5}, 2.5×10^{-5}, 5.0×10^{-5}, and 7.5×10^{-5} mol L^{-1} of the AB segment.

Preparation of Films of Cross-Linked Polymer Dyes. A polymer NP film (Chart 1) was prepared by copolymerization of NP (0.33, 0.67, or 1.34 mg) and *N*-isopropylacrylamide (0.68 g) with azobis(isobutyronitrile) (12 mg) and *N*,*N*′-methylenediacrylamide (81 mg) as a cross-linker in DMSO (3.0 mL) at 60 °C for 8 h following injection of the solution into a rectangular space. The rectangular space was located between two pieces of glass with a 2 cm × 2 cm hollowed-out Teflon spacer (thickness 0.5 mm) between them. All of the prepared films were immersed in methanol for 2 days and then in water for 2 days. The supernatant solution became clear, and the absence of reactants was verified by UV−vis spectroscopy. The obtained polymer NP films with different NP contents (NP1, NP2, and NP3) were measured by UV−vis absorption spectroscopy to determine the molar concentration u (mol L^{-1}) of NP under the assumption that each polymer NP film (film area: 4 cm^2) was dissolved in 4 mL of water; the measured molar concentrations were 3.5×10^{-5} mol L^{-1} (NP1), 6.2×10^{-5} mol L^{-1} (NP2), and 1.1×10^{-4} mol L^{-1} (NP3).

A polymer AB film (Chart 1) was prepared by copolymerization of AB (0.075, 0.12, 0.15, or 0.30 mg) with *N*-isopropylacrylamide (0.68 g), azobis(isobutyronitrile) (12 mg), and *N*,*N*′-methylenediacrylamide (81 mg) in DMSO

https://doi.org/10.1021/acsomega.4c05320
ACS Omega 2024, 9, 36682−36689

Chart 1. Structure of the Polymer Dye Films

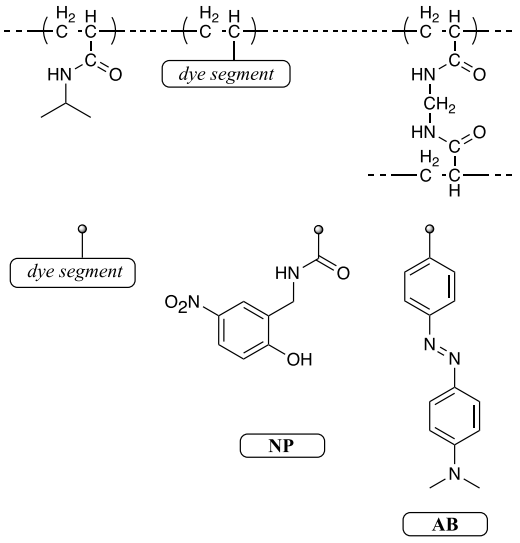

(3.0 mL) at 60 °C for 8 h in the same glass case used to prepare the polymer NP films. The obtained polymer AB films with different AB contents—AB1, AB2, AB3, and AB4—were similarly characterized by UV−vis absorption spectroscopy to determine u (mol L^{-1}) of AB under the assumption that each polymer AB film (area of the film: 4 cm^2) was dissolved in 4 mL of water; the measured molar concentrations were 1.3×10^{-5} mol L^{-1} (AB1), 2.7×10^{-5} mol L^{-1} (AB2), 3.5×10^{-5} mol L^{-1} (AB3), and 7.3×10^{-5} mol L^{-1} (AB4).

Measurements of Solution Color of the Polymer Dyes and the Polymer Dye Films. Buffer solutions with various pH values were prepared using hydrochloric acid, sodium hydride, $NaHPO_4$, and NaH_2PO_4. The pK_a values of the polymer dye films were calculated using the absorbance change at the wavelength of maximum absorbance (320 nm for polymer NP and 520 nm for polymer AB). The polymer dye films were measured not only with a diode-array spectrophotometer (8453, Agilent) but also with a spectrocolorimeter (MV-3200, JASCO) using a halogen illuminant (LUS-361, JASCO) in which a D65 lamp was used as a light source. The color information for the polymer dye films was captured in the form of CIELAB ($L^*a^*b^*$) and CIE XYZ data. The synthesized polymeric dye films were cut and immersed in buffers with different pH values as shown in Figure S1. The coordinates at which the chromaticity point obtained by colorimetry became constant after immersion were the observation points, and the color transition of the polymer dye film was determined using these trajectories. The response time of the color change of the polymeric NP and AB films to reach equilibrium at each pH, which depended on pH, was within a few minutes. Planarity with the mixture of the chromaticity points for AB1 and AB2 was statistically analyzed by the least-squares method using Mathematica 14.0 (Wolfram Research).

RESULTS AND DISCUSSION

Transition of Chromaticity Points in the CIELAB Color Space upon Protonation of Polymeric NP. The polymeric NP films (NP1, NP2, and NP3) immersed in water neither swelled nor leaked the NP dye into the surrounding water, enabling stable pH monitoring over a long period. The polymeric NP films were transparent over the entire pH range, colorless in the acidic range, and yellow in the alkaline range (Scheme 1).

Scheme 1. Reversible Protonation of NP as a Dye Portion of the Polymer NP

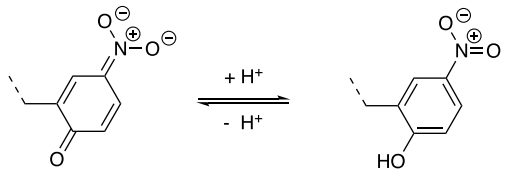

deprotonated form of NP (yellow, λ_{max} 430 nm)

protonated form of NP (no color, λ_{max} 320 nm)

Figure 1 shows that NP2 reversibly changed between the protonated and deprotonated forms of NP in response to pH

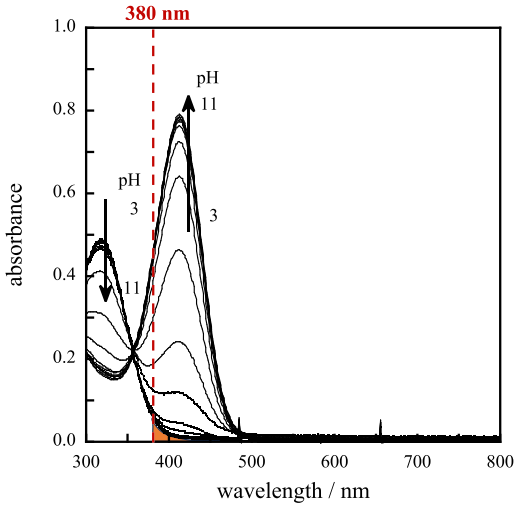

Figure 1. Absorption spectra of NP2 as the pH of the aqueous solution is varied from 3 to 11 in increments of 0.5.

changes, as evident in the absorption bands (λ_{max} = 320 and 430 nm for the protonated and deprotonated forms, respectively) with an isosbestic point (360 nm). A slight shoulder at wavelengths longer than 380 nm (orange area in Figure 1) remained on the long-wavelength side of the 320 nm absorption band in the visible region, even in an acidic solution at pH 3.0, where the colorless protonated form was dominant. However, the CIELAB chromaticity points exhibited by the other polymeric NP films, as well as those exhibited by the NP2 film, at pH 3.0 corresponded to nearly colorless, with $a^* \approx b^* \approx 0$ (square plots in Figure 2a). Figure 2b,c shows nearly unchanged lightness $L^* \approx 100$ for all of the polymeric NP films, indicating that the lightness difference, ΔL^*, between the chromaticity points that changed upon protonation of the NP is negligible. Therefore, the color difference, ΔE^*_{ab}, between the measured chromaticity point and the white point, $(a^*, b^*, L^*) = (0, 0, 100)$, in all of the polymer NP films can be regarded as the two-dimensional Euclidean distance between the observed chromaticity point and the origin in the a^*b^* coordinate plane.

In the polymeric NP films immersed in an aqueous solution at pH 11, almost all of the NP dye moieties were deprotonated and the yellow color of the films reached saturation (Figure 1). The transition of the chromaticity points for the dominant deprotonated NP with increasing concentration of NP showed

https://doi.org/10.1021/acsomega.4c05320
ACS Omega 2024, 9, 36682−36689

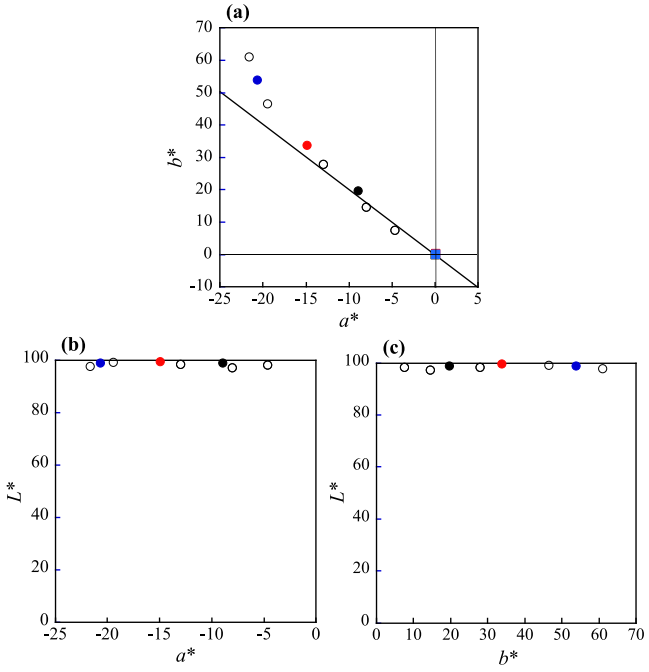

Figure 2. (a) a^*b^*-, (b) a^*L^*-, and (c) b^*L^*-projected chromaticity points of the polymer NP films (NP1 (black), NP2 (red), and NP3 (blue)) in aqueous solution at pH 12.5 (circles) and 3.0 (squares). The white circled points represent solutions of un-cross-linked polymer NP with different NP concentrations. The straight line was obtained from eq 2.

a linear locus (eq 2) from the origin (the white point) to $(a^*, b^*) = (-13, -28)$ (Figure 2a). This result indicates that perceptual linearity is limited in a low NP concentration range ($<4.7 \times 10^{-5}$ mol L^{-1}) because the Abney effect is avoided.

$$b^* = -2.0 \times a^* \tag{2}$$

Figure 3a shows the correlation between the concentration of NP in the polymeric NP films, u, and their color difference ΔE^*_{ab} from the white point. Figure 3b,c shows the correlations between u and a^* and between u and b^*, respectively. From the correlations, stoichiometric linearity in the CIELAB color space, which must satisfy stoichiometry in all aspects of the variables (a^*, b^*, and L^*) with u, holds for NP concentrations less than 4.7×10^{-5} mol L^{-1}. This range is the same as the linear locus of the chromaticity points in the a^*b^* coordinates shown in Figure 2a, matching the effective range of perceptual linearity and stoichiometric linearity. The consequent equation including u as the NP concentration and α as a protonation ratio ($0 \le \alpha \le 1$) of NP, eq 3 from Figure 3b,c, can be presented on the basis of stoichiometric linearity in the limited line in the CIELAB color space: $-13 \le a^* \le 0$, $0 \le b^* \le 28$, and $L^* \simeq 100$.

$$\begin{pmatrix} a^* \\ b^* \\ L^* \end{pmatrix} = (1-\alpha)\begin{pmatrix} -3.0 \times 10^5 \\ 6.0 \times 10^5 \\ 0 \end{pmatrix} u + \begin{pmatrix} 0 \\ 0 \\ 100 \end{pmatrix}$$

$$0 \le \alpha \le 1, \quad u \le 4.7 \times 10^{-5}\ (\mathrm{mol/L}) \tag{3}$$

Transition of Chromaticity Points in the CIELAB Color Space upon Protonation of Polymeric AB. Similar to the polymeric NP films, the polymeric AB films maintained their shapes without swelling in water over the entire investigated pH range. Under weakly acidic conditions (pH 5.0), AB was yellow

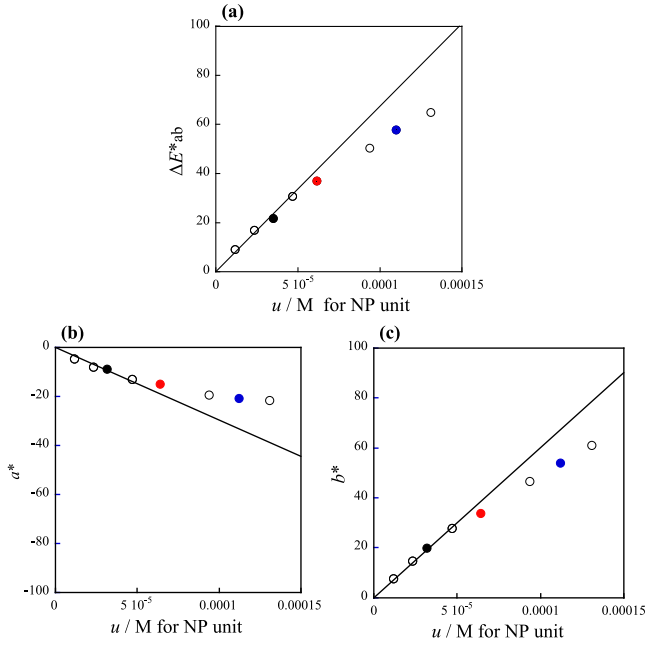

Figure 3. Correlation of (a) ΔE^*_{ab}, (b) a^*, or (c) b^* and the NP concentration, u, for the polymer NP films (NP1 (black), NP2 (red), and NP3 (blue)) in aqueous solution at pH 12.5. Other points are for solutions of the un-cross-linked polymer NP.

(λ_{max} = 450 nm), whereas under strongly acidic conditions (pH 0.5), the dominant protonated AB was red (λ_{max} = 520 nm) (Scheme 2 and Figure 4). The change in the absorption spectra upon protonation of AB displayed an isosbestic point at 490 nm (Figure 4), indicating that only AB protonation occurred.

Scheme 2. Reversible Protonation of AB as a Dye Portion of the Polymer AB

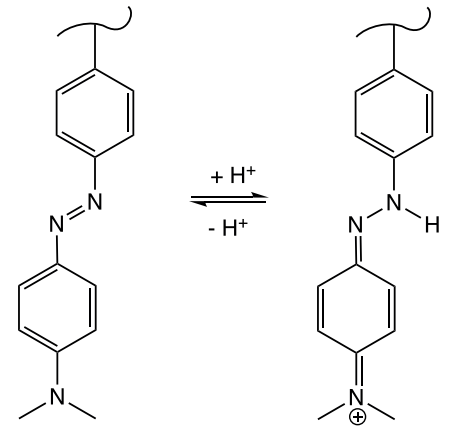

deprotonated form of AB (yellow, λ_{max} 450 nm)

protonated form of AB (red, λ_{max} 520 nm)

We calculated the pKa using the Henderson−Hasselbalch equation and the pH and absorbance data at 450 nm, where the band in the absorption spectrum is attributed to the deprotonated AB (Table 1). The same pK_a value of ∼2.7 ± 0.1 was obtained for all of the polymeric AB films, supporting the stoichiometric linearity between the absorbance indicated in the absorption spectra to the AB concentration in this concentration range, consistent with the Lambert−Beer rule.

https://doi.org/10.1021/acsomega.4c05320
ACS Omega 2024, 9, 36682−36689

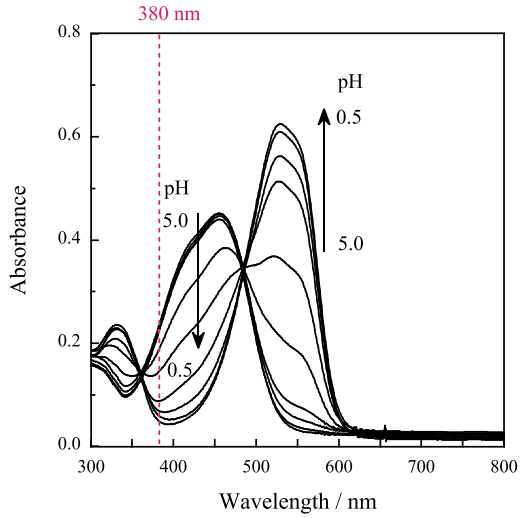

Figure 4. Absorption spectra of AB2 as the pH of the aqueous solution is increased from 0.5 to 5.0 in increments of 0.5.

Table 1. pK_a Values of the Polymer AB Films Calculated from the Absorption Spectra and ΔE^*_{ab} in the CIELAB Color Space

	pK_a	
polymer AB film	absorption spectra	ΔE^*_{ab}
AB1	2.7	2.8
AB2	2.6	2.6
AB3	2.8	2.8
AB4	2.6	2.7

Figure 5 shows that the chromaticity points for all of the polymeric AB films (AB1, AB2, AB3, and AB4) varied with pH in the CIELAB color space. AB1 and AB2, which had relatively low AB concentrations, had chromaticity points near the white point (a*, b^*, L^*) = (0, 0, 100), resulting in a flat approximated plane (eq 4, R^2 = 0.991) obtained by the least-squares method

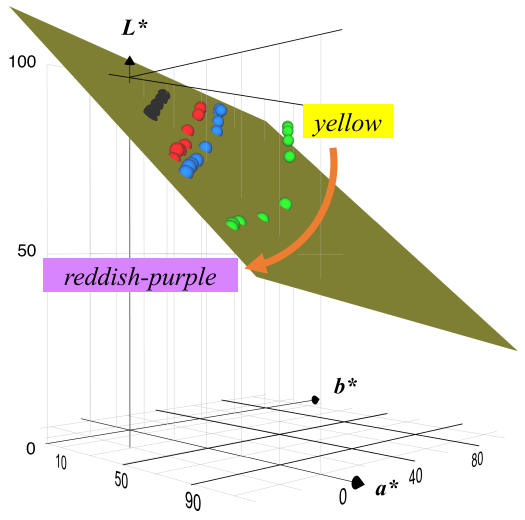

Figure 5. Transition of the chromaticity points in the CIELAB color space as the pH is varied for the polymer AB films (AB1 (black), AB2 (red), AB3 (blue), and AB4 (green)). The plane (eq 4) was calculated using least-squares regression with the points for the two films of AB1 and AB2.

with all chromaticity points for AB1 and AB2 varying with pH. As the pH was lowered from pH 5.0, all the polymer AB films changed from yellow to reddish-purple and their chromaticity points converged at pH 0.5, where protonated AB was dominant (Figure 4). The chromaticity points for all the films at pH 0.5 are on the plane, despite the large ΔE^*_{ab} from the substantive white point of the plane, (a^*, b^*, L^*) = (0, 0, 98). By contrast, at pH 5.0 in the yellow region, the chromaticity points for the dominant deprotonated AB of AB3 and AB4 exhibited a substantial departure from the plane. This departure was attributed to the reversal of the a^* increase/decrease in the high-saturation area for AB3 and AB4 with high AB concentrations.

$$L^* = -0.47a^* - 0.14b^* + 98 \quad (4)$$

In addition, the chromaticity point for only AB1 and AB2, which transitioned from yellow to red-purple as protonation of AB proceeded, showed linear loci with identical slopes (eq 5 for AB1 and eq 6 for AB2). The slopes of other loci of chromaticity points that transition upon protonation of AB were not identical and changed moderately for AB3 and dramatically for AB4. A steep change of the loci near a protonation ratio (α) of 0.5 for AB3 and AB4 indicates perceptual nonlinearity. From these results, the chromaticity points upon protonation of AB have a limited perceptually linear region, which includes the chromaticity points indicated by AB1 and AB2. This range constructs a triangular plane, the three vertices of which are the substantive white point, (0, 0, 98), the yellow point for the deprotonated AB for AB2, (−7.3, 45, 95), and the red-purple point for the protonated AB for AB2, (59, −21, 73), from the calculation using eq 6

$$b^* = -0.99a^* + 17 \ (R^2 = 0.999)$$
$$L^* = -0.32 \times a^* + 96 \ (R^2 = 0.986)$$
$$L^* = 0.32 \times b^* + 90 \ (R^2 = 0.988) \quad (5)$$

$$b^* = -1.0a^* + 38 \ (R^2 = 0.999)$$
$$L^* = -0.33a^* + 93 \ (R^2 = 0.993)$$
$$L^* = 0.32b^* + 81 \ (R^2 = 0.995) \quad (6)$$

Figure 6 shows the projection of the chromaticity points in Figure 5 onto two-dimensional coordinates in three different directions: a^*b^* (a), a^*L^* (b), and b^*L^* (c). In Figure 6a, the chromaticity points indicated by AB1 and AB2 at pH 5.0 are aligned in a straight line (l_{ab}) from the substantive white point, (a^*, b^*) = (0, 0), suggesting perceptual linearity in this range. The extension of the line l_{ab} to the range of AB4 gives the pale-blue circled point as a virtual chromaticity point, assuming perceptual linearity extending to AB4. The measured chromaticity points shown by AB4 at pH 5.0 from this virtual chromaticity point are shifted positively in a^* and negatively in b^*. This shift, which caused the deviation from the approximate plane in Figure 5, is likely due to the pronounced Abney effect resulting from the increased saturation. In the CIE 1931 xy coordinates in Figure S2, the point for AB4 is red-shifted from the linear locus (l_{xy}) of the chromaticity points in the low-AB-concentration region, suggesting this effect. Similarly, the chromaticity points indicated by AB1 and AB2 at pH 5.0 are on the straight lines l_{aL} and l_{bL} in Figure 6b,c, respectively, whereas the chromaticity points indicated by AB4 deviate substantially from these lines.

https://doi.org/10.1021/acsomega.4c05320
ACS Omega 2024, 9, 36682−36689

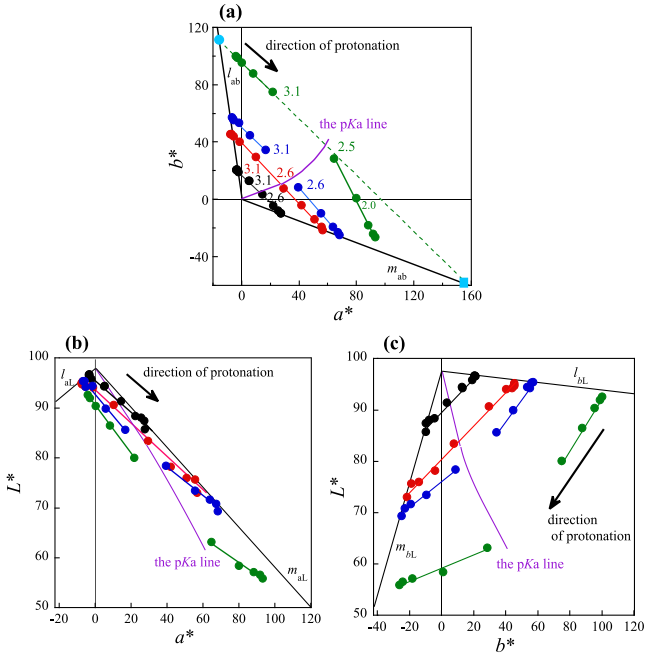

Figure 6. (a) a^*b^*-, (b) a^*L^*-, or (c) b^*L^*-projected chromaticity points of the polymer AB films with various AB concentrations as the pH change of the aqueous solutions is varied from 5.0 to 4.6, 4.1, 3.6, 3.1, 2.6, 2.1, 1.6, 1.0, and 0.5 for the black points (AB1); from 5.0 to 4.5, 4.1, 3.6, 3.1, 2.6, 2.1, 1.6, 1.1, and 0.6 for the red points (AB2); from 5.0 to 4.6, 4.1, 3.5, 3.1, 2.6, 2.1, 1.6, 1.0, and 0.6 for the blue points (AB3); and from 5.0 to 4.4, 4.0, 3.5, 3.1, 2.5, 2.0, 1.5, 1.0, and 0.5 for the green points (AB4).

In the region of predominantly protonated AB at pH 0.5, the chromaticity points indicated by the polymeric AB films, except for AB4, are on the straight line m_{ab} (Figure 6a). The deviation of AB4 from this straight line is likely attributable to the Bezold–Brücke phenomenon that occurs in color spaces with a pronounced reduction in lightness reaching nearly 50 (Figure 6b,c).[25] The locus comprising the chromaticity points for the initial stage of AB protonation in AB4 is extended as a dotted line in Figure 6a. The intersection (a pale-blue squared point) of the dotted line and line m_{ab} is the virtual chromaticity point, where the perceptual linearity from the yellow region is assumed to continue into the red-purple region. The direction from the chromaticity point to the observed chromaticity point can be estimated as the direction of the hue shift due to the Bezold–Brücke phenomenon. In Figure 6b,c, the observed chromaticity points are shifted to a larger L^* because of this phenomenon, suggesting that the low lightness that cannot be detected effectively by cones can be captured by highly sensitive rods.

Stoichiometrically Linear Transition of Chromaticity Points for the Deprotonated and the Protonated AB with AB Concentration. The color difference ΔE^*_{ab} between the chromaticity point indicated by the polymeric AB and the substantive white chromaticity point in aqueous solutions at pH 5.0 and 0.5 is correlated with the concentration of AB, u, as shown in Figure 7a,b, respectively. In contrast to the absorption spectra results, ΔE^*_{ab} is proportional to u only at AB concentrations less than 2.7×10^{-5} mol L^{-1} in the solutions with different pHs (5.0 and 0.5) in cases where AB1 and AB2 were included; ΔE^*_{ab} deviated from the proportional line slightly in the case of AB3 and noticeably in the case of AB4. Here, we denote the ΔE^*_{ab} between the chromaticity point at the dominant protonated AB in the films and the substantive white point as ΔE^*_{ab}(pro). We also denote theΔE^*_{ab} between the point at the dominant deprotonated AB and the substantive white point as ΔE^*_{ab}(de). Subtracting ΔE^*_{ab}(de) from ΔE^*_{ab}(pro) (i.e., ΔE^*_{ab}(pro) − ΔE^*_{ab}(de)) gives a result that corresponds to the ΔE^*_{ab} in which all AB segments in the films change upon protonation. Because the pKa is the pH of an aqueous solution with equal concentrations of protonated and deprotonated species (in this case, AB ($\alpha = 0.5$)), the pK_a of the polymeric AB films can be calculated using ΔE^*_{ab}(pro) − ΔE^*_{ab}(de) by substituting for the corresponding change in absorbance of the absorption spectra, followed by Henderson–Hasselbalch analysis. Table 1 shows that the pKa values obtained from the calculation closely agree with the pK_a values calculated from the absorption spectra. The results show that the CIELAB color space appears to exhibit perceptual color uniformity for all the polymeric AB films in terms of ΔE^*_{ab}, which incorporates all three components (a^*, b^*, and L^*). This result is partly attributable to the values of ΔE^*_{ab}(pro) and ΔE^*_{ab}(de) for AB3 and AB4 both being smaller than those in the proportional lines for lower AB concentrations (Figure 7a,b). The sequent loci of the chromaticity points for AB3 and AB4 were curved in the CIELAB color space, and stoichiometric linearity was no longer present in the region including AB3 and AB4 (i.e., a region corresponding to a high AB concentration).

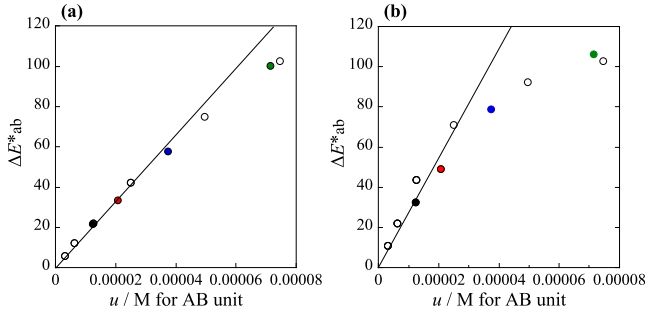

Figure 7. Correlation of ΔE^*_{ab} and concentration of AB, u, for the polymeric AB films. AB1 (black), AB2 (red), AB3 (blue), and AB4 (green) in aqueous solution at (a) pH 5.0 and (b) 0.5. Other points are for solutions with different concentrations of the un-cross-linked polymer AB.

The correlations at pH 5.0 between each component (a^*, b^*, and L^*) of the CIELAB color space and u emphasize this behavior, except for L^* (Figure 8a–c). Stoichiometric linearity, which is determined on the basis of the correlation between each of the three components and the AB concentration in the deprotonated form, is only applicable for AB1 and AB2. The valid range for the stoichiometric linearity for the deprotonated AB is on a straight line (eq 7) in the range $-7 \le a^* \le 0$, $0 \le b^* \le 45$, $95 \le L^* \le 100$, which includes AB1 and AB2.

$$a^* = -2.9 \times 10^5 u$$
$$b^* = 1.7 \times 10^6 u$$
$$L^* = -2.0 \times 10^5 u + 98$$
$$u \le 2.7 \times 10^{-5}\ (\text{mol/L}) \quad (7)$$

Similarly, the correlations at pH 0.5 between each component and u of the protonated AB in Figure 9a–c shows that the stoichiometric linearity in the CIELAB color space is valid in the red-purple range as well as for the 2.7×10^{-5} mol L^{-1} AB in the protonated form for AB1 and AB2. The stoichiometric linearity in the red-purple region is supported by an approximately

https://doi.org/10.1021/acsomega.4c05320
ACS Omega 2024, 9, 36682−36689

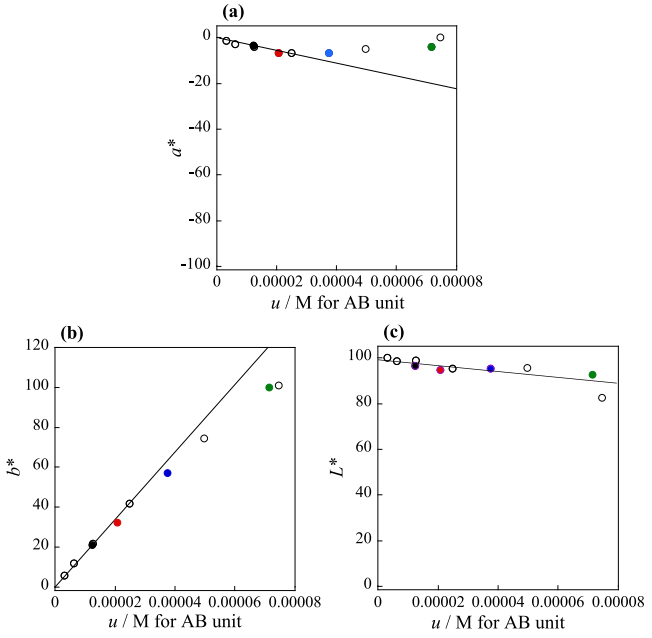

Figure 8. Correlation of (a) a^*, (b) b^*, or (c) L^* with the AB concentration (u) for the polymeric AB (AB1 (black), AB2 (red), AB3 (blue), and AB4 (green)) in aqueous solutions at pH 5.0. Other points are related to the solution of the un-cross-linked polymeric AB.

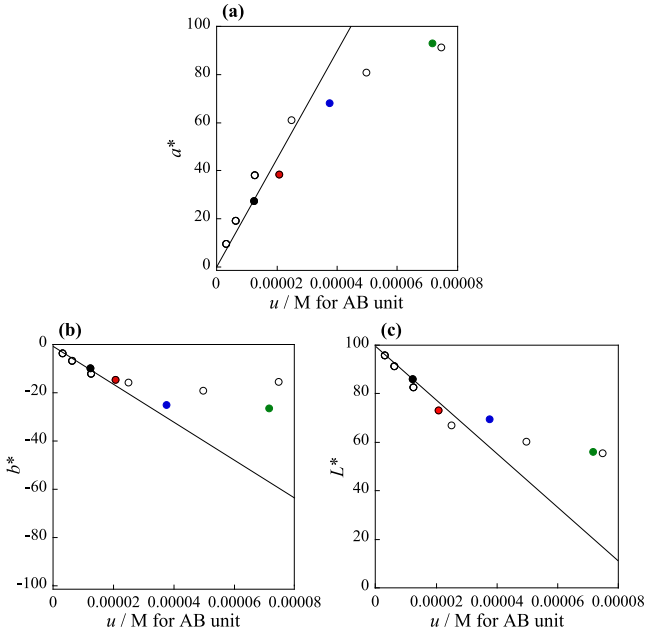

Figure 9. Correlation of (a) a^*, (b) b^*, or (c) L^* with the AB concentration (u) for polymeric AB (AB1 (black), AB2 (red), AB3 (blue), and AB4 (green)) in aqueous solutions at pH 0.5. Other points are related to the solution of the non-cross-linked polymeric AB.

straight line (eq 8) in the range $0 \le a^* \le 59, -21 \le b^* \le 0, 73 \le L^* \le 98$, which includes AB1 and AB2.

$$a^* = 2.2 \times 10^6 u$$
$$b^* = -8.0 \times 10^5 u$$
$$L^* = -1.0 \times 10^6 u + 98$$
$$u \le 2.7 \times 10^{-5}\ (\mathrm{mol/L}) \qquad (8)$$

Stoichiometrically Linear Region of Chromaticity Points Transitioning upon Protonation of Polymeric AB in the CIELAB Color Space. Stoichiometric linearity on the two triangle sides represented by eqs 7 and 8 includes the chromaticity points for AB1 and AB2, as mentioned above. Confirming stoichiometric linearity also inside the triangle requires a geometric approach in Euclidean space. The median line (the purple solid line in Figure 6) of the triangle from the substantive white point, which is a vertex connecting to two sides l_{ab} (or l_{aL} or l_{bL}) and m_{ab} (or m_{aL} or m_{bL}, respectively) of the triangle, intersects the opposite side, along which the chromaticity point transitions upon protonation of AB from the yellow into the reddish-purple region. This intersection is the theoretical chromaticity point, where the pH of the solution is equal to the pK_a of the polymeric AB films obtained by the geometric method, under the assumption that the limited space is stoichiometric. From AB1 to AB3, all such intersections are between pH 2.6 and 3.1 (Figure 6a); however, for AB4, the purple linear line should extend between the chromaticity points for solutions at pH 2.5 and 3.1, suggesting a pK_a theoretical line curvature similar to that of the purple-dotted line in the high-saturation region. These perceptual phenomena were likely caused by the high saturation and low lightness of AB4. According to the location of the observed chromaticity points of the polymeric AB immersed in a solution with a pH equal to the pK_a, in comparison with the intersection of the medium line from the substantive white point, the stoichiometric linearity likely holds in the triangle region in the CIELAB color space, leading to eq 9 for AB protonation when the AB concentration is less than 2.7×10^{-5} mol L^{-1}.

$$\begin{pmatrix} a^* \\ b^* \\ L^* \end{pmatrix} = \left\{ \alpha \begin{pmatrix} 2.2 \times 10^6 \\ -8.0 \times 10^5 \\ -1.0 \times 10^6 \end{pmatrix} + (1-\alpha) \begin{pmatrix} -2.9 \times 10^5 \\ 1.7 \times 10^6 \\ -2.0 \times 10^5 \end{pmatrix} \right\} u + \begin{pmatrix} 0 \\ 0 \\ 98 \end{pmatrix}$$
$$\alpha = \frac{1}{10^{\mathrm{pH}-\mathrm{p}K_a} + 1}$$
$$0 \le \alpha \le 1, \quad u \le 2.7 \times 10^{-5}\ (\mathrm{mol/L}) \qquad (9)$$

CONCLUSIONS

Both the polymeric NP and AB dyes exhibited yellow coloration in their deprotonated form and maintained high lightness, even at high dye concentrations. Thus, perception-specific nonlinear phenomena, such as the Abney effect, are less likely to occur, even at high saturation values. Stoichiometric linearity for the deprotonated form of NP and AB in the yellow region of the CIELAB color space is maintained at concentrations as high as 4.7×10^{-5} and 2.7×10^{-5} mol L^{-1}, respectively.

Upon protonation, the polymeric AB displayed loci consisting of the chromaticity points in the CIELAB color space from the yellow to the red-purple region upon protonation of AB and showed stoichiometric linearity at concentrations as high as 2.7×10^{-5} mol L^{-1} of AB in the red-purple region occupied by the protonated form of AB. In the restricted CIELAB color space, where stoichiometric linearity holds, eq 9 for the concentration of AB, u, and the protonation ratio of AB, α, allows for chromaticity points indicative of polymeric AB.

https://doi.org/10.1021/acsomega.4c05320
ACS Omega 2024, 9, 36682−36689

■ ASSOCIATED CONTENT

Supporting Information

The Supporting Information is available free of charge at https://pubs.acs.org/doi/10.1021/acsomega.4c05320.

Photographs, in which the color of the polymer NP and AB films varied reversibly with pH change; and transition of the chromaticity points of the polymer AB films in the CIE 1931 *xy* diagram (PDF)

■ AUTHOR INFORMATION

Corresponding Author

Takayuki Suzuki − *Department of Applied Chemistry, School of Engineering, Tokyo Denki University, Tokyo 120-8551, Japan*; orcid.org/0000-0003-2524-7133; Phone: +81-70-7667-9000; Email: suzutaka@cck.dendai.ac.jp

Authors

Chihiro Ito − *Department of Applied Chemistry, School of Engineering, Tokyo Denki University, Tokyo 120-8551, Japan*

Karen Kitano − *Department of Applied Chemistry, School of Engineering, Tokyo Denki University, Tokyo 120-8551, Japan*

Tomohiro Yamaguchi − *Department of Applied Chemistry, School of Engineering, Tokyo Denki University, Tokyo 120-8551, Japan*

Complete contact information is available at: https://pubs.acs.org/10.1021/acsomega.4c05320

Author Contributions

T.S. conceptualized the project; C.I., K.K., and T.Y. performed the experiments; T.S., C.I., and T.Y. analyzed the data; T.S. wrote the manuscript; T.S. and T.Y. revised the manuscript; T.S. supervised the project.

Funding

This work was supported in part by the Research Institute for Science and Technology of Tokyo Denki University (Grant Number Q22P-02/Japan).

Notes

The authors declare no competing financial interest.

■ ACKNOWLEDGMENTS

This work was supported by the TDU Analysis Center, Tokyo Denki University.

■ REFERENCES

(1) Capitán-Vallvey, L. F.; Lopez-Ruiz, N.; Martinez-Olmos, A.; Erenas, M. M.; Palma, A. J. Recent developments in computer vision-based analytical chemistry: A tutorial review. *Anal. Chim. Acta* **2015**, *899*, 23−56.

(2) Fernandes, G. M.; Silva, W. R.; Barreto, D. N.; Lamarca, R. S.; Gomes, P. C. F. L.; Petruci, J. F. D.; Batista, A. D. Novel approaches for colorimetric measurements in analytical chemistry - A review. *Anal. Chim. Acta* **2020**, *1135*, 187−203.

(3) Magubane, S. E.; Mlambo, M.; Mabaso, M. H.; Muthwa, S. F.; Kruger, H. G.; Mdluli, P. S. Optimization of CIEL*a*b*/Yxy colour system for colorimetric devices fabricated with gold nanoparticles. *J. Mol. Struct.* **2019**, *1191*, 271−277.

(4) Cantrell, K.; Erenas, M. M.; de Orbe-Paya, I.; Capitan-Vallvey, L. F. Use of the hue parameter of the hue, saturation, value color space as a quantitative analytical parameter for bitonal optical sensors. *Anal. Chem.* **2010**, *82*, 531−542.

(5) Ariza-Avidad, M.; Cuellar, M. P.; Salinas-Castillo, A.; Pegalajar, M. C.; Vukovic, J.; Capitán-Vallvey, L. F. Feasibility of the use of disposable optical tongue based on neural networks for heavy metal identification and determination. *Anal. Chim. Acta* **2013**, *783*, 56−64.

(6) Andrade, S. I. E.; Lima, M. B.; Barreto, I. S.; Lyra, W. S.; Almeida, L. F.; Araújo, M. C. U.; Silva, E. C. A digital image-based flow-batch analyzer for determining Al(III) and Cr(VI) in water. *Microchem. J.* **2013**, *109*, 106−111.

(7) Thanomsak, S.; Insombat, C.; Chaiyo, P.; Tuntulani, T.; Janrungroatsakul, W. Fabrication of a paper-based sensor from graphene quantum dots coated with a polymeric membrane for the determination of gold(III) ions. *Anal. Methods* **2021**, *13*, 4785−4792.

(8) Martínez-Olmos, A.; Fernández-Salmerón, J.; Lopez-Ruiz, N.; Torres, A. R.; Capitan-Vallvey, L. F.; Palma, A. J. Screen printed flexible radiofrequency identification tag for oxygen monitoring. *Anal. Chem.* **2013**, *85*, 11098−11105.

(9) Meier, R. J.; Schreml, S.; Wang, X. D.; Landthaler, M.; Babilas, P.; Wolfbeis, O. S. Simultaneous photographing of oxygen and pH in vivo using sensor films. *Angew. Chem., Int. Ed.* **2011**, *50*, 10893−10896.

(10) Komatsu, T.; Mohammadi, S.; Busa, L. S. A.; Maeki, M.; Ishida, A.; Tani, H.; Tokeshi, M. Image analysis for a microfluidic paper-based analytical device using the CIE L(star)a(star)b(star) color system. *Analyst* **2016**, *141*, 6507−6509.

(11) Wang, Y.; Liu, Y.; Liu, W.; Tang, W. H.; Shen, L.; Li, Z. L.; Fan, M. K. Quantification of combined color and shade changes in colorimetry and image analysis: water pH measurement as an example. *Anal. Methods* **2018**, *10*, 3059−3065.

(12) Shen, L.; Hagen, J. A.; Papautsky, I. Point-of-care colorimetric detection with a smartphone. *Lab Chip* **2012**, *12*, 4240−4243.

(13) Yetisen, A. K.; Martinez-Hurtado, J. L.; Garcia-Melendrez, A.; Vasconcellos, F. D.; Lowe, C. R. A smartphone algorithm with inter-phone repeatability for the analysis of colorimetric tests. *Sens. Actuators, B* **2014**, *196*, 156−160.

(14) Lopez-Ruiz, N.; Curto, V. F.; Erenas, M. M.; Benito-Lopez, F.; Diamond, D.; Palma, A. J.; Capitan-Vallvey, L. F. Smartphone-based simultaneous pH and nitrite colorimetric determination for paper microfluidic devices. *Anal. Chem.* **2014**, *86*, 9554−9562.

(15) Meier, R. J.; Schreml, S.; Wang, X. D.; Landthaler, M.; Babilas, P.; Wolfbeis, O. S. Simultaneous photographing of oxygen and pH in vivo using sensor films. *Angew. Chem., Int. Ed.* **2011**, *50*, 10893−10896.

(16) Sharma, G.; Wu, W. C.; Daa, E. N. The CIEDE2000 color-difference formula: Implementation notes, supplementary test data, and mathematical observations. *Color Res. Appl.* **2005**, *30*, 21−30.

(17) Wyszecki, G. Proposal for a new color-difference formula. *J. Opt. Soc. Am.* **1963**, *53*, 293−296.

(18) Eastwood, D. A simple modification to improve the perceptual uniformity of the CIE 1964 U*V*W* colour space. *Farbe* **1975**, *24*, 97−108.

(19) Abe, K.; Suzuki, K.; Citterio, D. Inkjet-printed microfluidic multianalyte chemical sensing paper. *Anal. Chem.* **2008**, *80*, 6928−6934.

(20) Alfvin, R. L.; Fairchild, M. D. Observer variability in metameric color matches using color reproduction media. *Color Res. Appl.* **1997**, *22*, 174−188.

(21) Robertson, A. R. The CIE 1976 Color-Difference Formulae. *Color Res. Appl.* **1977**, *2*, 7−11.

(22) Verhoeven, J. W. Glossary of terms used in photochemistry. *Pure Appl. Chem.* **1996**, *68*, 2223−2286.

(23) Levkowitz, H.; Xu, L. L. In *Approximating the Munsell Book of Color with the Generalized Lightness, Hue, and Saturation Color Model*, Color Hard Copy and Graphic Arts; SPIE, 1992; pp 325−334.

(24) Ohta, N. Structure of the color solid obtainable by three subtractive color dyes. *Die Farbe* **1971**, *20*, 115−134.

(25) Judd, D. B.; Wyszecki, G. Extension of the Munsell renotation system to very dark colors. *J. Opt. Soc. Am.* **1956**, *46*, 281−284.